Seasonal prediction of boreal winter stratosphere

A. Portal (UNIMIB)[+], P. Ruggieri (UNIBO), F. Palmeiro, J. Garcia-Serrano (UB), D. Domeisen (ETH Zürich), S. Gualdi (CMCC)

[+] Contact information: Alice Portal, University of Milan-Bicocca (DISAT), a.portal@campus.unimib.it

Motivations:

I. Measuring the winter predictability of the stratosphere in 5 Copernicus seasonal prediction models initialised in November[1].

II. Assessing model reproduction of the coupling between lower-stratosphere wave forcing (**LSWF**) and stratosphere polar vortex (**SPV**). See schematics of Figure 1.

III. Determining the impact of local-LSWF forecast skill on SPV skill.

Coupling between LSWF and SPV, **diagnostics**:

LSWF $\longleftrightarrow$ $\langle \overline{v'T'} \rangle_{100}$, 100-hPa Eliassen–Palm flux (vertical component) average in 40-80° N

SPV $\longleftrightarrow$ $\overline{U}_{10}$[55-70N], 10-hPa zonal-mean zonal wind average in 55-70° N

where $'$: deviation from zonal mean
$\bar{\cdot}$: zonal mean
$\langle \cdot \rangle$: meridional mean in mid latitudes

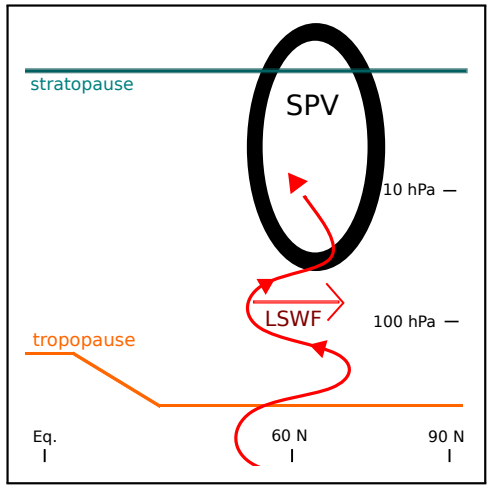

Figure 1: Waves propagating upwards from the troposphere (LSWF) break in the SPV and decelerate it. Latitude–pressure perspective.

[1] See description of the models in "Additional material 1"

Seasonal predictability of the boreal stratosphere

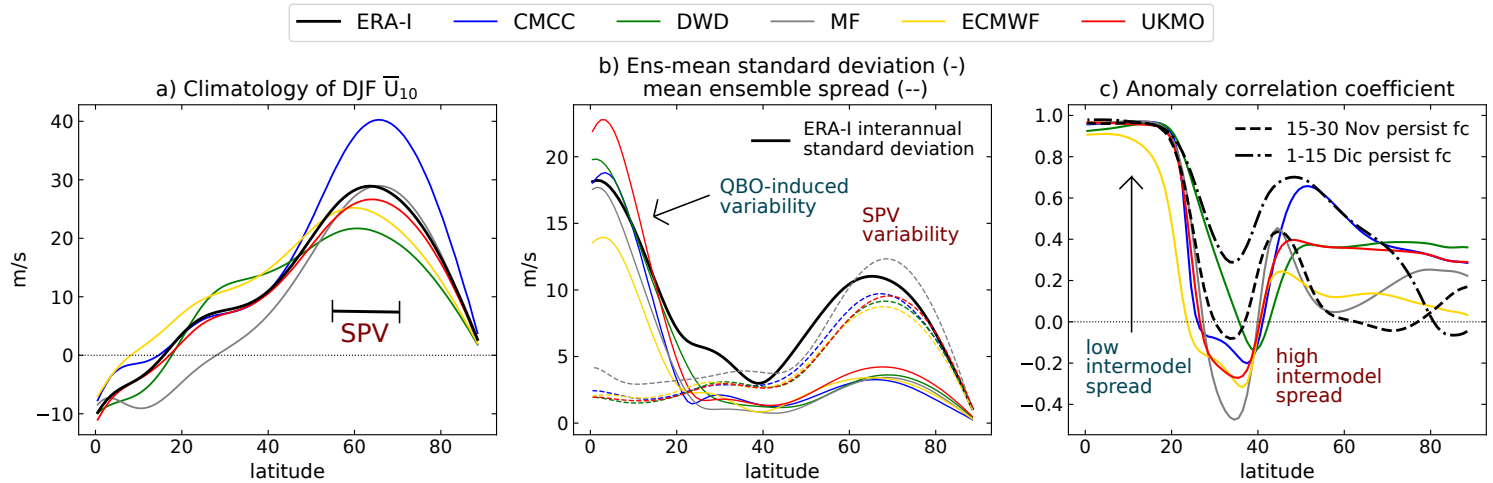

Figure 2: **Variability and predictability of December-January-February (DJF) stratosphere, function of latitude**. DJF averages of zonal-mean zonal wind at 10 hPa are used to compute: **a**) 1993/94-to-2016/17 climatology; **b**) ensemble-mean or interannual standard deviation (solid), mean spread of the model ensemble (dashed); **c**) correlation coefficient between ensemble-mean and ERA-Interim anomalies.

- Seasonal variability and predictive skill are affected by *tropical* QBO and *extratropical* SPV.
- The *tropics* are well predicted due to the longer QBO timescale compared to the seasonal scale.
- The *extratropics* are less predictable due to low signal-to-noise ratio (ens. mean std/mean ens. spread, Figure 2b). Observe the wide inter-model spread in the *extratropical* predictive skill. The skill does not depend on SPV model bias (cf. panels a and c in Figure 2).
- Low predictive skill in the *subtropics* may affect the propagation of the *tropical* QBO in the *extratropics* (Holton–Tan mechanism).

Seasonal predictability of the boreal stratosphere

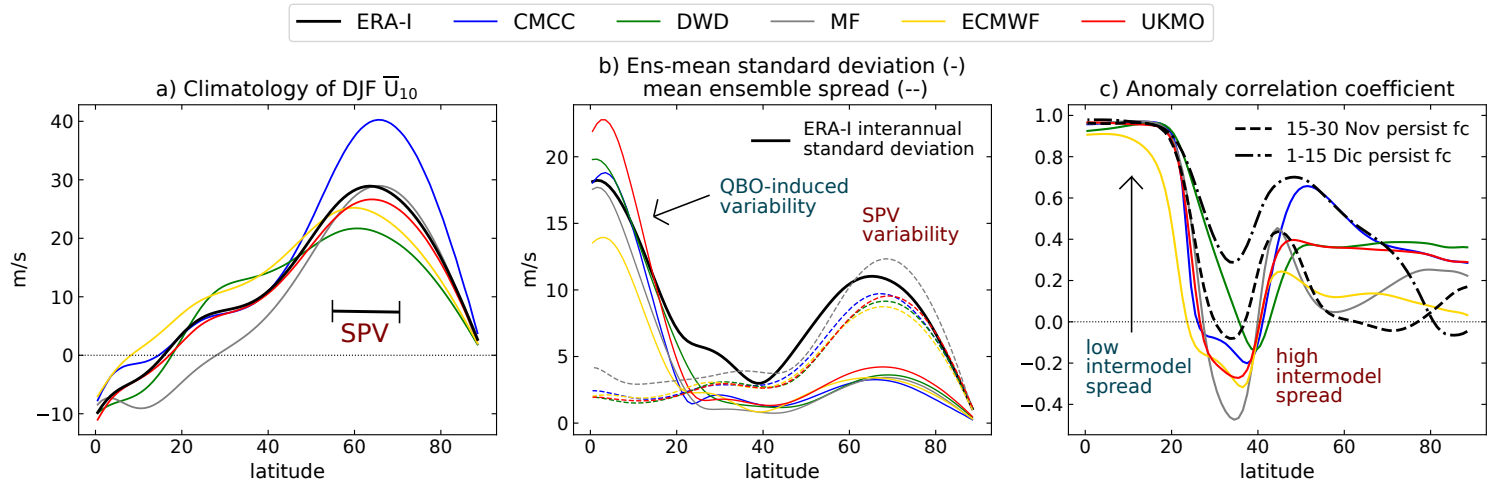

Figure 2: **Variability and predictability of December-January-February (DJF) stratosphere, function of latitude**. DJF averages of zonal-mean zonal wind at 10 hPa are used to compute: **a**) 1993/94-to-2016/17 climatology; **b**) ensemble-mean or interannual standard deviation (solid), mean spread of the model ensemble (dashed); **c**) correlation coefficient between ensemble-mean and ERA-Interim anomalies.

Stratospheric polar vortex:

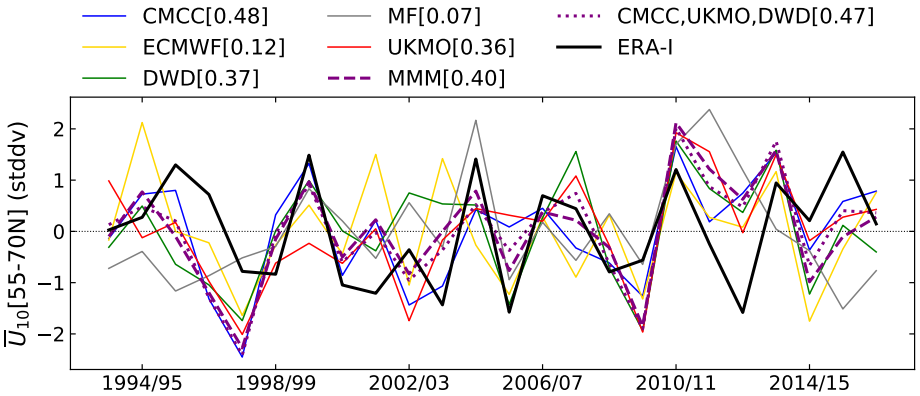

Three models (CMCC, DWD, UKMO) show significant winter predictive skill for the SPV.
We look at monthly skill values...

Figure 3: **Ensemble-mean/interannual variability of the DJF SPV**, seasonal model ACC in label.

Seasonal predictability of the boreal stratosphere

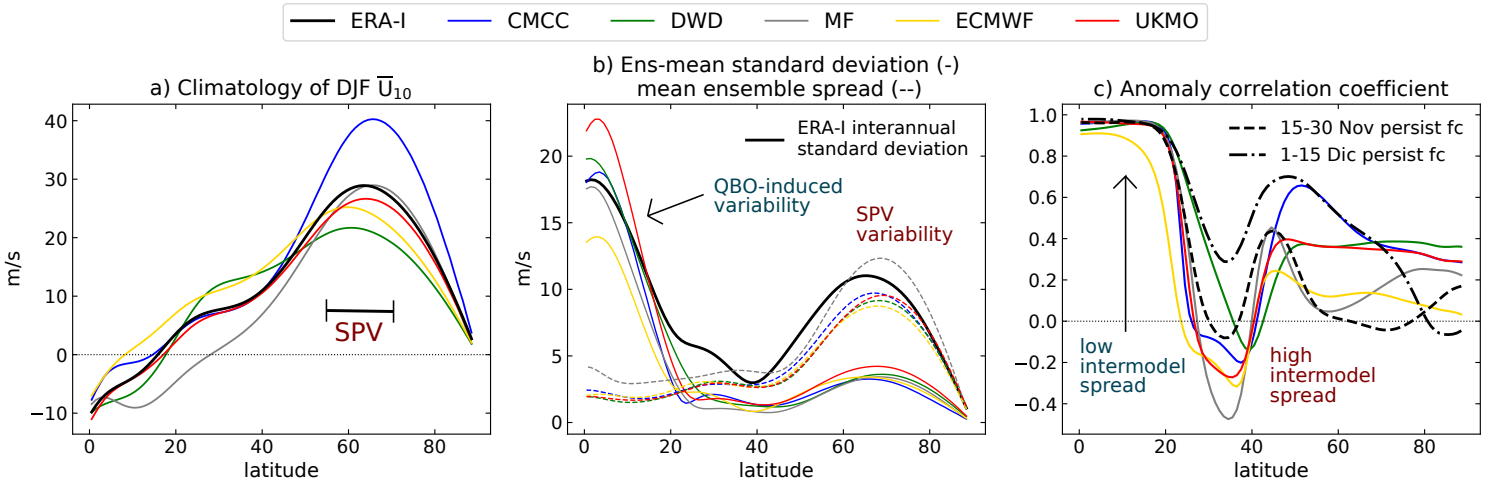

Figure 2: **Variability and predictability of December-January-February (DJF) stratosphere, function of latitude**. DJF averages of zonal-mean zonal wind at 10 hPa are used to compute: **a**) 1993/94-to-2016/17 climatology; **b**) ensemble-mean or interannual standard deviation (solid), mean spread of the model ensemble (dashed); **c**) correlation coefficient between ensemble-mean and ERA-Interim anomalies.

Stratospheric polar vortex:

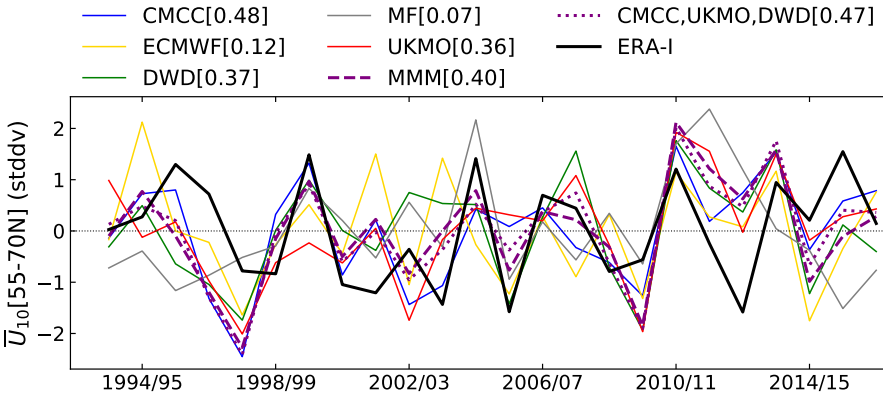

Figure 3: **Ensemble-mean/interannual variability of the DJF SPV**, seasonal model ACC in label.

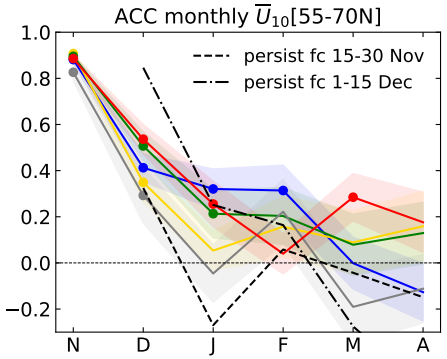

Figure 4: **Monthly ACC** and its standard deviation (shading, from bootstrap). Full dots evidence significant skill ($p \leq 0.05$).

Relation between SPV and LSWF

We define a reconstruction of the SPV-wind anomaly ($\Delta\overline{U}_{10}$) on the basis of previous LSWF anomalies [2]

$$\Delta\overline{U}^{*}_{10}(t) \equiv -\mathcal{B} \underbrace{\int_{t_0}^{t} \Delta\langle\overline{v'T'}\rangle_{100}(t_f)\, e^{-(t-t_f)/\tau}\, dt_f}_{\text{integral of time-weighed LSWF anomalies}}, \tag{1}$$

with $\tau = 45$ days, $\mathcal{B}$ constant.

Following, we assess the relation between SPV and LSWF on daily and seasonal time scale: the effective SPV-wind anomaly, $\Delta\overline{U}_{10}$, is displayed against the correspondent anomaly reconstructed from LSWF, $\Delta\overline{U}^{*}_{10}$. Slope and correlation values, computed for each scatter plot, facilitate the comparison between model LWSF–SPV coupling and ERA-Interim coupling.

[2] derived from "*Relation between the 100-hPa Heat Flux and Stratospheric Potential Vorticity*", Hinssen and Ambaum (2010)

Relation between SPV and LSWF

Reconstruction of the SPV-wind anomaly ($\Delta\overline{U}_{10}$) from previous LSWF anomalies [3]

$$\Delta\overline{U}^{*}_{10}(t) \equiv -\mathcal{B}\int_{t_0}^{t} \Delta\langle\overline{v'T'}\rangle_{100}(t_f)\, e^{-(t-t_f)/\tau}\, dt_f$$

Figure 5: **Daily assessment**. Density of the scatter plot between daily values of SPV wind anomaly, $\Delta\overline{U}_{10}$, and of its reconstruction from LSWF anomalies, $\Delta\overline{U}^{*}_{10}$.

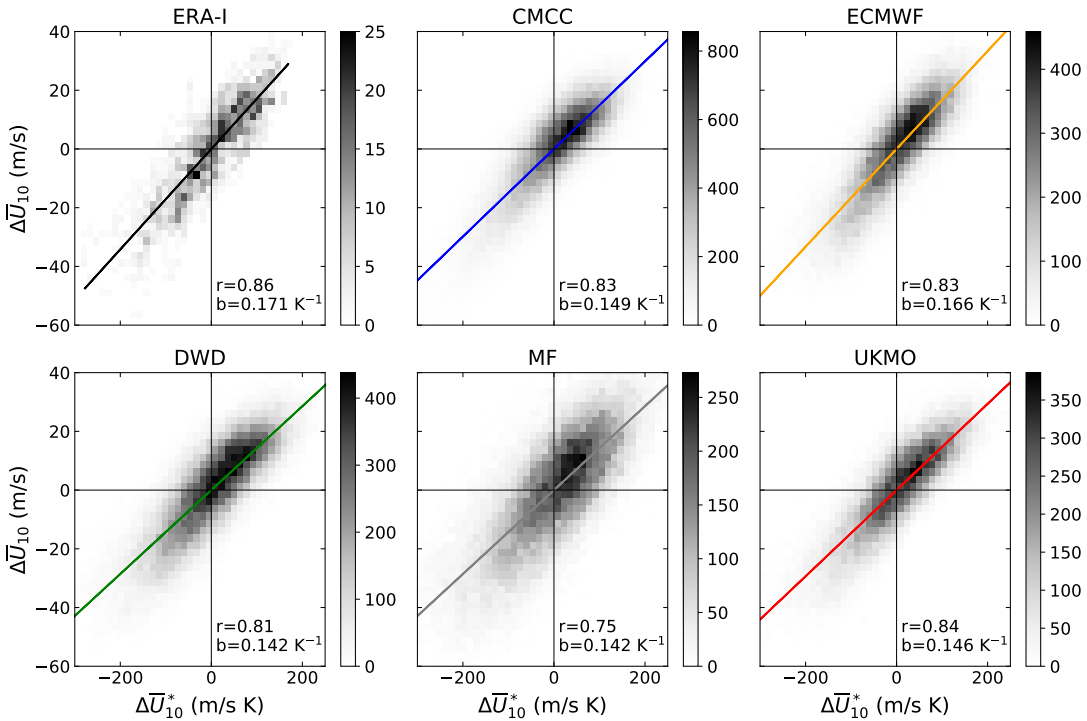

- Discrepancies from ERA-Interim distribution are found mainly in CMCC (too narrow) and MF (too wide).
- In MF, LSWF is not as determinant for the SPV as is found in reanalysis. This is evidenced by reduced model correlation (r).
- All models display weaker coupling between LSWF and SPV compared to reanalysis (see values of b and r).

[3] derived from "*Relation between the 100-hPa Heat Flux and Stratospheric Potential Vorticity*", Hinssen and Ambaum (2010)

Relation between SPV and LSWF

Reconstruction of the SPV-wind anomaly ($\Delta\overline{U}_{10}$) from previous LSWF anomalies [4]

$$\Delta\overline{U}^{*}_{10}(t) \equiv -\mathcal{B}\int_{t_0}^{t} \Delta\langle\overline{v'T'}\rangle_{100}(t_f)\, e^{-(t-t_f)/\tau}\, dt_f$$

- Models with higher skill in predicting the DJF SPV also show stronger interannual variability of LSWF ($\Delta\overline{U}^{*}_{10}$).
- One model (DWD) reproduces a weaker link between interannual variability of LSWF and of SPV, as shown by model r_{DJF}.
- ERA-Interim seasonal coupling between LSWF and SPV is generally stronger than in models (see values of b_{DJF} and r_{DJF}).

Figure 6: **Seasonal assessment**. Scatter plot between DJF (ensemble-mean) values of SPV wind anomaly, $\Delta\overline{U}_{10}$, and of its reconstruction from LSWF anomalies, $\Delta\overline{U}^{*}_{10}$.

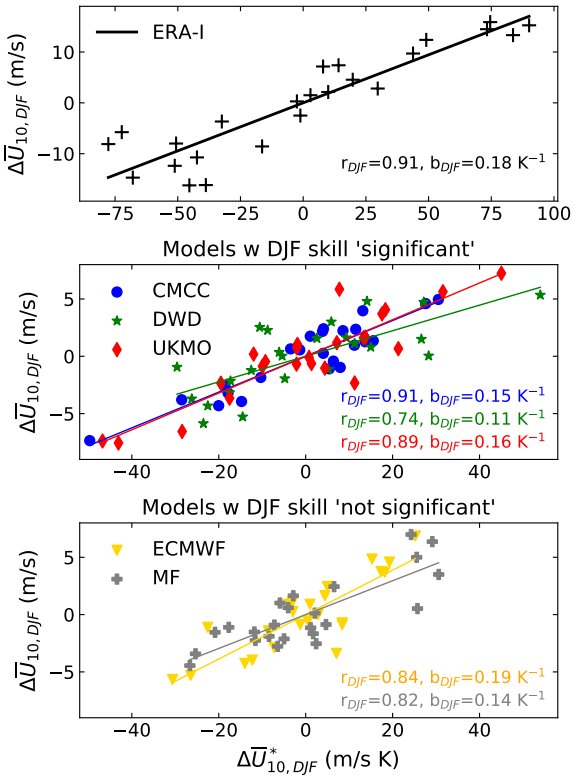

[4] derived from "*Relation between the 100-hPa Heat Flux and Stratospheric Potential Vorticity*", Hinssen and Ambaum (2010)

Predictability of local LSWF ($v'T'$), links with ENSO

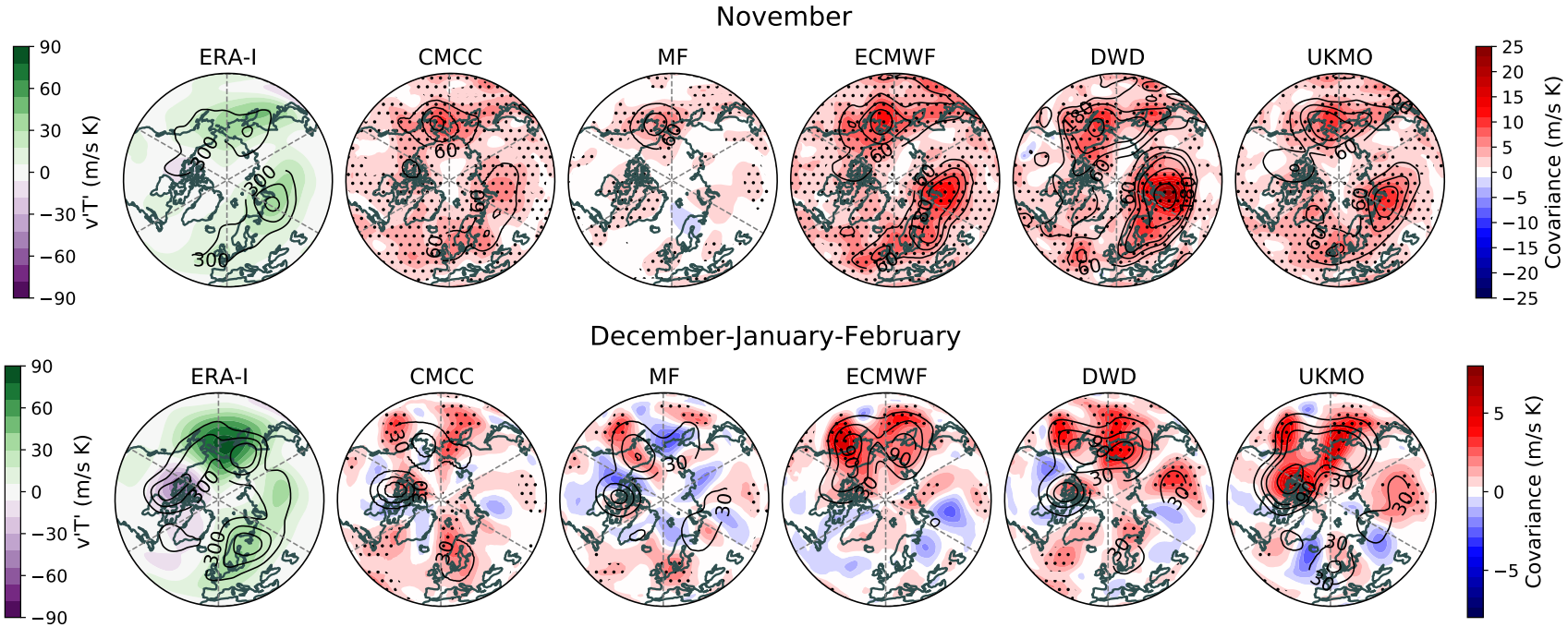

Figure 7: **Left**: ERA-Interim climatologies of $v'T'$ (green–purple). **Right**: Covariance between model ensemble mean $v'T'$ and standardised ERA-Interim $v'T'$ (blue–red, note different scaling in November and DJF). Stippling shows significant ACC ($p \leq 0.05$). Black contours show model ensemble-mean variance at 60, 120, 180, 300, 600 $(m/s\ K)^2$ in November; at 30, 60, 90, 180 $(m/s\ K)^2$ in DJF; reanalysis interannual variance at 300, 600, 900 $(m/s\ K)^2$.

- The predictive skill for November is good in all models exept MF.
- Residual DJF model skill is found mainly in the Pacific sector. It is lower and model-dependent over Eurasia.

We inquire the local-LSWF response to ENSO in models and in reanalysis, in order to understand whether seasonal Pacific predictability is related to ENSO.

The impact of other potential sources of seasonal stratospheric predictability (QBO, Arctic sea-ice extent and Eurasian snow cover) is considered in "Additional material 2".

Predictability of local LSWF ($v'T'$), links with ENSO

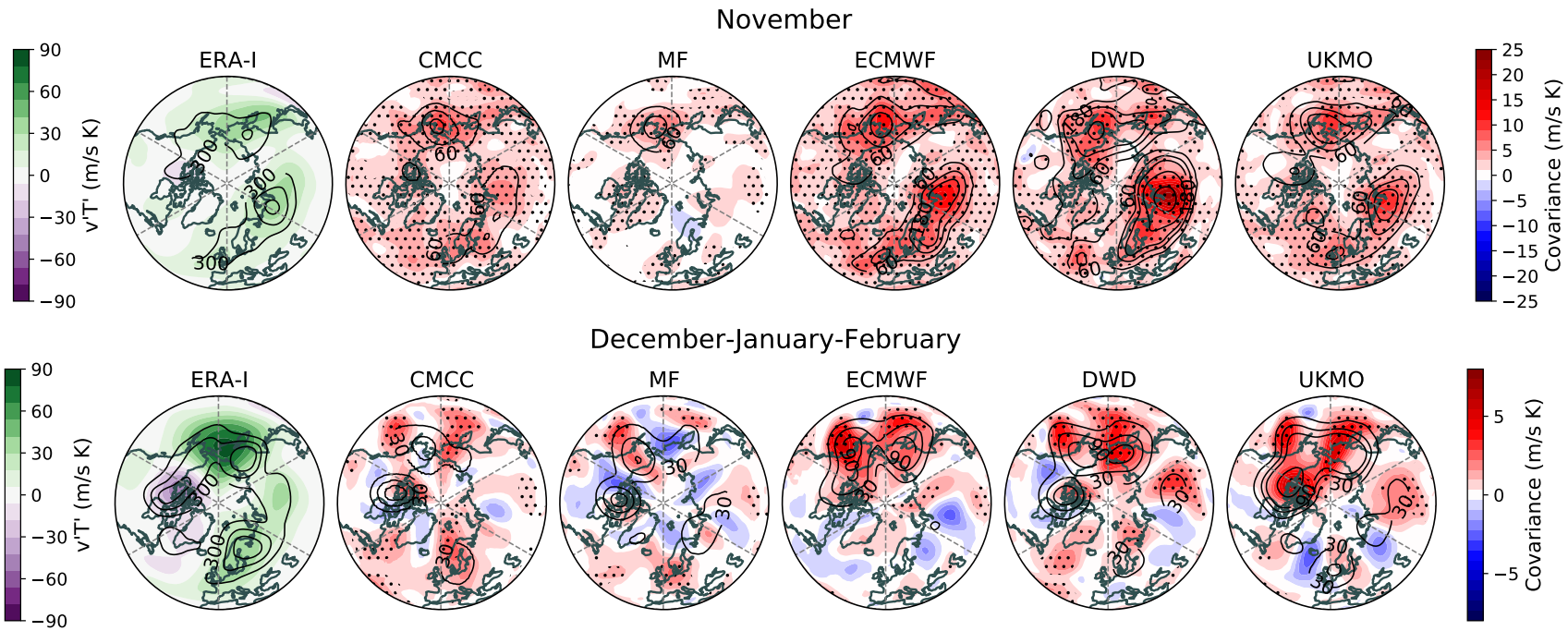

Figure 7: **Left**: ERA-Interim climatologies of $v'T'$ (green–purple). **Right**: Covariance between model ensemble mean $v'T'$ and standardised ERA-Interim $v'T'$ (blue–red, note different scaling in November and DJF). Stippling shows significant ACC ($p \leq 0.05$). Black contours show model ensemble-mean variance at 60, 120, 180, 300, 600 $(m/s\ K)^2$ in November; at 30, 60, 90, 180 $(m/s\ K)^2$ in DJF; reanalysis interannual variance at 300, 600, 900 $(m/s\ K)^2$.

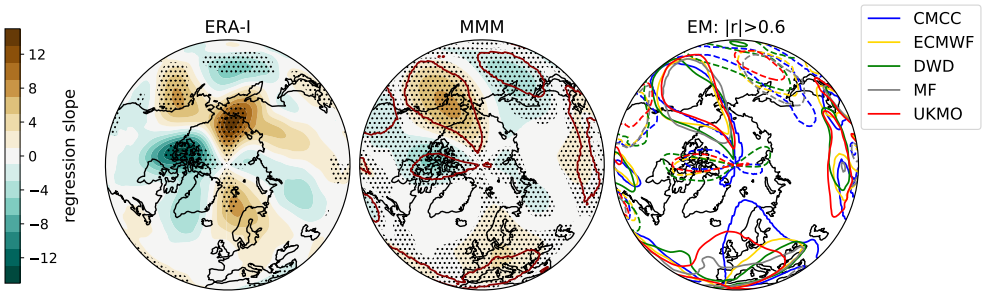

Figure 8: **Impact of ENSO on local LSWF**. regression of $v'T'$ on niño3.4 index—DJF averages—for ERA-Interim (**left**) and for multi-model mean (MMM, **center**). In the latter, total model agreement in the sign of the regression is highlighted with dark red contours. Correlation (r) between model ensemble-mean $v'T'$ and niño3.4 is displayed for values greater/smaller than 0.6/-0.6 (EM, **right**).

Relation between regional LSWF and SPV

Predictability of regional LSWF:

- West- and East- North Pacific LSWF displays seasonal skill, mainly thanks to ENSO (cf. Figure 7 and 8);
- Eurasian LSWF shows high interannual variance, but is poorly predictable in the seasonal range (Figure 7).

We estimate the importance of Pacific and Eurasian LSWF for the seasonal variability of the SPV. Model results are compared with reanalysis.

Table 1: **Strength of the link between SPV and regional LSWF**. Correlation between DJF anomalies of SPV winds ($\Delta\overline{U}$) and DJF wind anomalies reconstructed from regional LSWF ($\Delta\overline{U}^{*}_{\text{reg}}$, see Eq. 1). The latter are calculated using $v'T'$ from the regions selected in the figure on the right. Bold values are significant at 95% confidence level.

	40-80° N	W Pacific	E Pacific	Pac sec	Eurasia
CMCC	**0.91**	-0.05	**0.75**	**0.40**	**0.85**
MF	**0.82**	-0.33	**0.61**	**0.55**	**0.51**
ECMWF	**0.84**	-0.22	**0.53**	0.26	**0.71**
DWD	**0.74**	**-0.35**	**0.45**	0.07	**0.69**
UKMO	**0.89**	**-0.40**	**0.68**	0.19	**0.64**
ERA-I	**0.91**	0.14	0.01	0.11	**0.72**

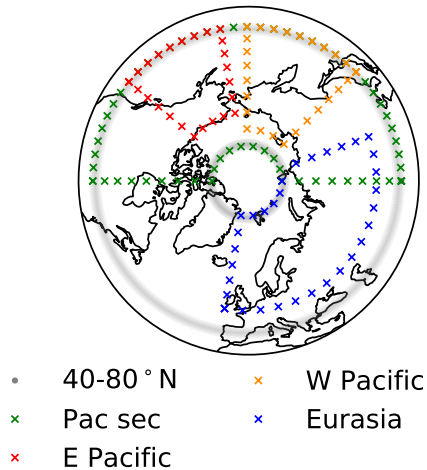

Summary of the results

I. In the boreal stratosphere:
   - winter variability and predictability are affected by QBO in the tropics and by the presence of the SPV in the extratropics (Figure 2);
   - we find a wide inter-model spread in the winter predictability of the SPV, which does not depend on bias. Three models exhibit significant DJF skill (Figures 3, 4).

II. Daily coupling between LSWF and SPV is well reproduced by 4 models (Figure 5). One model, MF, shows substantial departures from reanalysis.
Seasonal anomalies of LSWF explain $\sim 80\%$ of interannual SPV variability (Figure 6). One model, DWD, shows weaker seasonal coupling.

III. Good predictability of the local LSWF is found within a month from initialisation (Nov). Over the Pacific model skill persists into DJF, it is weaker over Atlantic and Eurasia.
Model SPV skill is favoured by:
   - strong interannual variability of the winter LSWF (Figure 6);
   - November predictability of local LSWF (Figure 7);
   - DJF predictability of Eurasian LSWF (Table 1), lacking in models that exhibit no SPV skill in the seasonal range (Figure 7).

Model SPV shows a strong link with regional Pacific LSWF (Table 1) forced by strong SPV–ENSO teleconnection (Figure 8). This feature is not present in reanalysis.

Additional material 1

General description of the 5 seasonal prediction systems.

Models	Resolution *	Initial Conditions **	Ensemble Size
CMCC (system 3)	1° lat/long 46 L	1st November	40 members
MF (system 6)	TL359 91 L	20th, 25th October 1st November	2×12 members 1 member
ECMWF (SEAS5)	$T_{CO}319$ 91 L	1st November	25 members
DWD (system 2)	T127 95 L	1st November	30 members
UKMO (GloSea5, system 13)	N216 95 L	25th October 1st, 9th November	7 members for start date

*For vertical resolution we indicate the number of vertical levels (L).
**Model simulations start on the 1st of November, in years 1993 to 2016. Differently, UKMO simulations start on three separate dates between the end of October and the beginning of November—see initial-conditions dates.

Additional material 2

Impact of seasonal winter signal on LSWF and SPV:

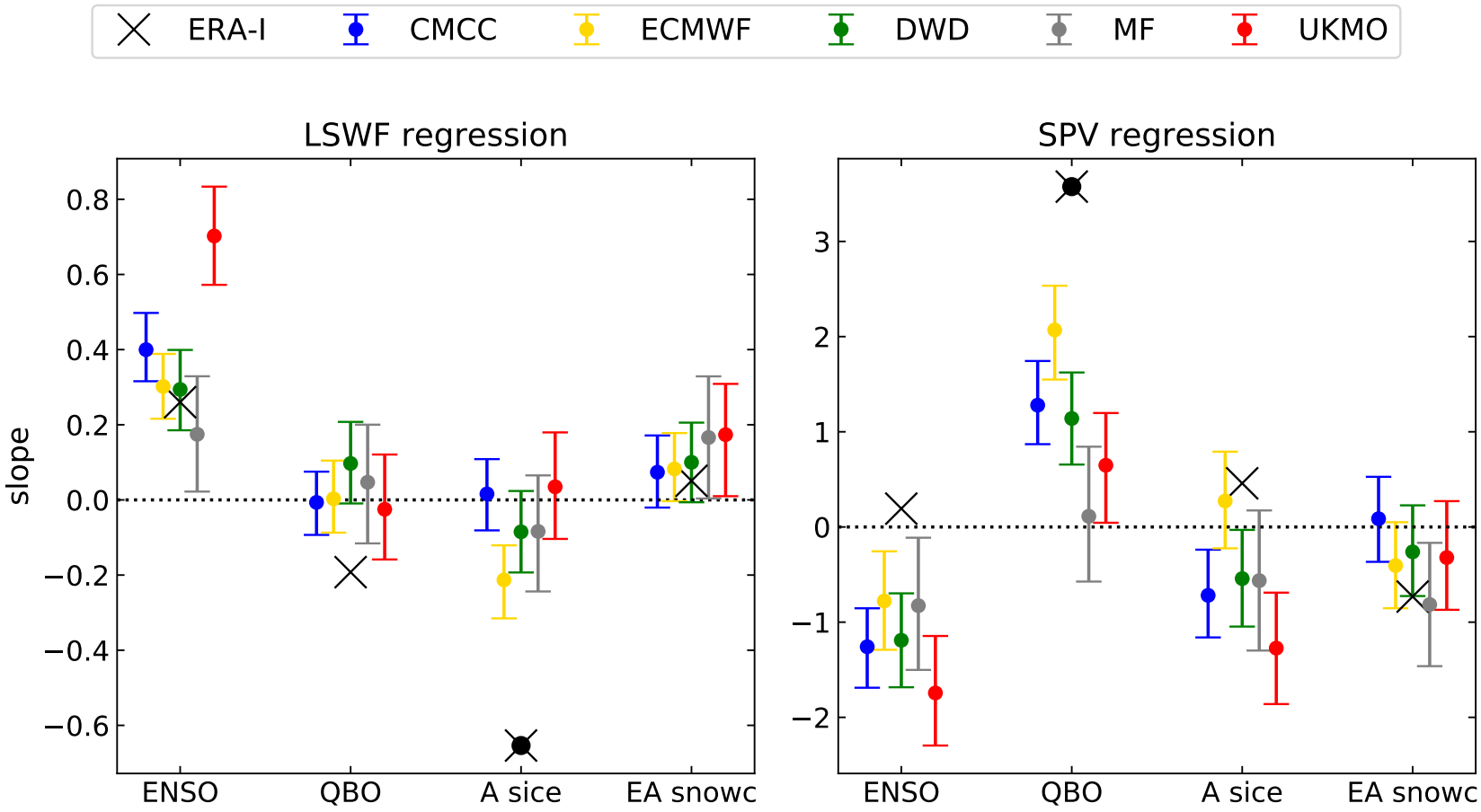

Figure 9: **Regressions on sources of seasonal variability**. On the left, the linear regression slope between DJF LSWF and seasonal signals, i.e. DJF ENSO, DJF QBO, October-November Arctic sea ice, October-November Eurasian snow cover. The same for DJF SPV on the right. The 5th and 95th percentile of model slope are represented with errorbars—relative distribution is calculated using bootstrap. ERA-Interim regressions characterised by significant correlation according to one-tailed t-test ($p \leq 0.05$) are indicated with full black circles on top of black crosses.